CMLS, Cell. Mol. Life Sci. 61 (2004) 1082–1094
1420-682X/04/091082-13
DOI 10.1007/s00018-004-3469-5

CMLS Cellular and Molecular Life Sciences

Research Article

Myelination in the hippocampus during development and following lesion

S. Meier [a], A. U. Bräuer [a], B. Heimrich [a, b], R. Nitsch [a] and N. E. Savaskan [a, c, *]

[a] Institute of Cell Biology and Neurobiology, Center for Anatomy, Charité University Medical School Berlin, Philippstr. 12, 10115 Berlin (Germany), Fax: +49 30 450 528 902, e-mail: nicolai.savaskan@charite.de
[b] Institute of Anatomy and Cell Biology I, Albert-Friedrichs University of Freiburg (Germany)
[c] Present address: Division of Cellular Biochemistry, The Netherlands Cancer Institute, Plesmanlaan 121, 1066 OX Amsterdam (The Netherlands), e-mail: n.savaskan@kki.nl

Received 22 December 2003; received after revision 11 February 2004; accepted 17 February 2004

Abstract. Myelin is crucial for the stabilization of axonal projections in the developing and adult mammalian brain. However, myelin components also act as a non-permissive and repellent substrate for outgrowing axons. Therefore, one major factor which accounts for the lack of axonal regeneration in the mature brain is myelin. Here we report on the appearance of mature, fully myelinated axons during hippocampal development and following entorhinal lesion with the myelin-specific marker Black Gold. Although entorhinal axons enter the hippocampal formation at embryonic day 17, light and ultrastructural analysis revealed that mature myelinated fibers in the hippocampus occur in the second postnatal week. During postnatal development, increasing numbers of myelinated fibers appear and the distribution of myelinated fibers at postnatal day 25 was similar to that found in the adult. After entorhinal cortex lesion, a specific anterograde denervation in the hippocampus takes place, accompanied by a long-lasting loss of myelin. Quantitative analysis of myelin and myelin breakdown products at different time points after lesion revealed a temporally close correlation to the degeneration and reorganization phases in the hippocampus. In contrast, electroconvulsive seizures resulted in brief demyelination and a faster recovery time course. In conclusion, we could show that the appearance of mature axons in the hippocampus is temporally regulated during development. In the adult hippocampus, demyelination was found after anterograde degeneration and also following seizures, suggesting that independent types of insult lead to demyelination. Reappearing mature axons were found in the hippocampus following axonal sprouting. Therefore, our quantitative analysis of mature axons and myelination effectively reflects the readjusted axonal density and possible electrophysiological balance following lesion.

Key words. Myelin-associated axon growth inhibition; Nogo gene; seizure; axonal guidance; myelo-architecture; myelin basic protein; sprouting; demyelination.

Neurons of the adult central nervous system (CNS) generally exhibit the capacity for axonal outgrowth in a permissive environment [1]. However, unlike the peripheral nervous system (PNS), the adult CNS suffers from a lack of recovery after injury [2–4]. In contrast to the growth-promoting Schwann cells of the PNS, myelin-forming oligodendrocytes form a non-permissive environment for axonal growth and regeneration [5–7]. There are several known myelin-derived proteins, which show axon growth-inhibitory properties limiting anatomical and functional recovery. Such molecules are myelin-associ-

* Corresponding author.

ated glycoprotein (MAG) [8, 9], oligodendrocyte-myelin glycoprotein (Omgp) [10], chondroitin sulfate proteoglycans (CSPGs) [11, 12], and the newly identified Nogo family [13–15]. However, the multilamellar, spirally wrapped structure originating from oligodendrocytes is also necessary for the proper functioning of mature axons [16, 17]. This specialized structure surrounding axons serves as an axonal insulator and reduces the energy and space expenditure of nerve cells. Therefore, considering the role of myelin in pathological processes of limited axonal regeneration requires a deeper understanding of its regional distribution in the brain.

In this study, we investigated the process of myelination in the hippocampus, a region known for its high structural plasticity during development and following lesion [18]. The perforant path, the main excitatory input to the hippocampus, originates from stellate and pyramidal cells of the entorhinal cortex and segregates layer specifically in the stratum lacunosum-moleculare of the cornu ammonis (CA) and in the outer molecular layer of the dentate gyrus (DG). During development, entorhinal fibers first reach the DG at embryonic day 19 (E19) [19]. The perforant path is almost formed at postnatal day 5 (P5). In the hippocampus, expression of the major myelin proteins MAG and myelin basic protein (MBP), which are restricted to mature oligodendrocytes, starts around P10 and is completed in the adult at P60 [20].

Transection of the perforant path via entorhinal cortex lesion (ECL) results in an anterograde degeneration of entorhinal fibers in the DG and in the CA regions of the hippocampus [21]. This process is followed by reactive sprouting of non-lesioned fibers and changes in myelin pattern [for reviews see refs 22, 23]. In another model linked to rapid entorhinal cortex stimulation, electroconvulsive seizures (ECS) induce structural and functional changes in neuronal connectivity and lead to glial activation and oligodendrocytic cell death [24–29].

Although many studies have focused on axonal pathfinding and sprouting in the hippocampus, few have investigated the process of myelination and its distribution in this area of the brain [20, 30–34]. Here we used the myelin-specific marker Black Gold, MBP and MAG-specific antibodies, as well as another marker commonly used for myelin, Luxol Fast Blue (LFB), to investigate the time course of myelination in the hippocampus during postnatal development at the level of single fibers. In addition, two lesion paradigms (transection vs seizures) were investigated in this study with emphasis on the time course of myelin breakdown products and the reoccurence of myelinated fibers. Our data extend knowledge concerning the appearance of myelinated fibers in the hippocampus during development, which exhibits temporal regulation and commences long after the expression of surrogate markers for mature oligodendrocytes [35]. In addition, we provide ultrastructural evidence for the presence of a high density of myelinated axons in the hilar region, which has, to our knowledge, otherwise only been indicated by immunolight microscopy [32]. Furthermore, we studied the disappearance and reappearance of myelinated fibers after axotomy and seizure on a quantitative level. In addition, as Black Gold selectively stains degenerating axons in the brain, our data support the sequence of axonal sprouting following lesion and record not only a subset of axons but all regrowing myelinated axons.

Materials and methods

Animals and surgery

In the present study, adult male Wistar rats (200–300 g body weight), housed under standard laboratory conditions, received a unilateral electrolytic lesion to the entorhinal cortex (ECL) [see also refs 36, 37]. All surgical procedures were performed in agreement with the German and European Law on the use of laboratory animals (Federal Contract Ni-344). Brains from postnatal rats on day 5 (n = 3), 12 (n = 5), 17 (n = 4) and 25 (n = 4) were perfused and brains immersion fixed overnight at 4 °C. The next day, brains were cryoprotected in 20% sucrose dissolved in 4% paraformaldehyde (PFA) for two days at 4 °C. For stereotactic surgery, rats were deeply anesthetized with a mixure of Ketanest (Gödecke/Parke-Davis, Freiburg, Germany), Rompun (Bayer, Leverkusen, Germany), and Ventranquil (Sanofi-Ceva, Düsseldorf, Germany) in 0.9% sterile NaCl and placed in a stereotactic head holder (Stoelting, Wood Dale, Ill.). A standard electrocoagulator was used to make unilateral incisions [with four single pulses (2.5 µA), 3 s each] in the frontal and sagittal planes between the entorhinal cortex and hippocampus. We used the following coordinates measured from lambda: frontal incision: AP + 1.2; L + 3.1 to + 6.1; V down to the interior of the cranium; sagittal incision: AP + 1.2 to + 4.2; L 6.1; V down to the interior of the cranium [38]. Rats were allowed to survive for 2, 5, 10, 28 and 60 days (± 0.5 days; three lesioned animals at each time). Three adult untreated animals served as controls.

For ECS, animals were deeply anesthetized as described above. Saline-soaked earclips were attached and with the help of the UGO Basile ECT unit (Milan, Italy), a stimulus of 1-s 100-Hz, 85-mA, 0.5-ms square-wave pulses was applied. This was repeated five times. After each set of stimuli, the rats exhibited generalized tonic-clonic convulsions with hindlimb extension. Animals were allowed to survive for 1 or 5 days.

The animals were deeply anesthetized with an overdose of the anesthetic mixture described above and transcardially perfused with 200 ml saline followed by 250 ml fixative. The animals used for the Black Gold staining

were fixed with 4% PFA and 0.1% or 2% glutaraldehyde dissolved in 0.1 M phosphate buffer, pH 7.5 (PB). The brains were postfixed in 20% sucrose dissolved in 4% PFA solution for 2 days and thereafter shock-frozen in the gaseous phase of liquid nitrogen and stored at –80 °C. Animals used for immunocytochemistry were transcardially perfused with 4% PFA in 0.1 M PB, with 0.1% glutaraldehyde serving as fixative for the Fluoro-Jade staining. Brains were removed and immerse-fixed overnight in the same fixative. Both for immunocytochemistry and Fluoro-Jade staining, horizontal serial sections of the entorhino-hippocampal region were cut on a vibratome at 50 µm for immunocytochemistry and 30 µm for Fluoro-Jade staining [38, 39]. Cryocut sections (30–50 µm) were used for Black Gold labeling.

Animals used for LFB staining were decapitated, and brains were immediately removed, frozen in the gaseous phase of liquid nitrogen, and stored at –80 °C. The thickness of the cryocut slices varied from 20 to 50 µm for optimal staining results and for detecting the entire axonal course.

Protein digestion

Sections used for the Black Gold staining were incubated with 50 µg/ml Proteinase K (Boehringer, Mannheim, Germany) dissolved in 0.01 M Tris (pH 8.0) and 0.1% SDS or with 0.25% Trypsin (Gibco, Karlsruhe, Germany) dissolved in dilution buffer containing KCl, $NaHCO_3$, NaCl and glucose at 37 °C for 40 min. Sections were afterwards stained with Black Gold and LFB.

Black Gold staining

A 0.2% solution of Black Gold (Histo-Chem, Jefferson, A.) was made by adding 20 mg of Black Gold to 10 ml of 0.9% NaCl and then briefly boiled in a microwave oven. For full equilibration, the solution was stored in the dark at 4 °C for at least 2 days. Frozen sections were collected in 0.1 PB. The mounted or free-floating sections were Black Gold stained at 60 °C in a conventional oven for about 30 min. The staining was intensified by incubation in a solution of 0.2% potassium tetrachloroaureate (Sigma-Aldrich, Taufkirchen, Germany) dissolved in 0.9% NaCl for 15 min at 60 °C. For fixation, the sections were incubated for 3 min in 2% sodium thiosulfate (Merck, Darmstadt, Germany) solution. At this point, the same adult sections were counterstained to localize the cell bodies. These sections were stained for 1.5 min in a 0.1% acetic acid solution of 0.4% malachite green (Sigma-Aldrich). The sections were rinsed in distilled water for 1 min and differentiated in 70% ethanol to remove background staining. Between each step, the sections were carefully rinsed in 0.1 M PB (three times, 5 min each). Finally, the free-floating sections were mounted on SuperFrostPlus slides (Menzel-Glaeser, Berlin, Germany), air dried, dehydrated in graded ethanol, cleared in xylene, and coverslipped with Entellan (both from Merck).

LFB staining

The freshly frozen tissue was postfixed in –20 °C cold methanol for 2 min and afterwards rinsed in an ethanol/acetic acid mixture (96/4%) for 5 min. Sections were incubated in 0.1% LFB solution dissolved in an ethanol/acetic acid mixture (96/4%) at 60 °C for 3 h. Sections were rinsed afterwards in 96% ethanol, postfixed in 0.05% Li_2CO_3 for 1 min, and washed in 70% ethanol for a few seconds. The sections were then counterstained with Harris Hematoxylin for 1–2 min. Sections were dehydrated in graded ethanol and coverslipped.

Immunocytochemistry for MBP and MAG

The sections were pretreated with 0.3% H_2O_2 followed by 10% normal horse serum (NHS). Sections were then incubated with the primary antibodies anti-MBP or anti-MAG (Boehringer) diluted 1:500 in PB containing 1% NHS, 0.1% NaN_3 and Triton X-100 or anti-MAG diluted 1:100 [see also ref. 20] for 48 h at 4 °C. This was followed by incubation in biotinylated antimouse IgG (Vector Laboratories, Burlingame, Calif.) diluted 1:250 in PB for 2 h at 20 °C, and developed with avidin-biotin peroxidase complex (ABC) reagent (Vectastain ABC-Kit, Vector Laboratories) diluted 1:100 in PB for 1.5 h at 20 °C. The immunoreaction was visualized with 3,3-diaminobenzidine (DAB) as a chromogen (0.07% DAB and 0.002% hydrogen peroxide in PB for 10 min). Between each incubation step, the sections were carefully rinsed five times for 10 min in PB. Finally, the sections were placed on SuperFrost slides, dehydrated in graded ethanol, and coverslipped.

Electron microscopy

For ultrastructural studies, Black Gold sections were osmicated (1% OsO_4 in 6.84% sucrose/PB for 5 min), dehydrated in graded ethanol, and flat embedded in Epon between silane-coated slides as described earlier [36, 40]. Ultrathin sections were cut on a Reichert Ultratome, mounted on single-slot grids coated with Formvar film, and stained with lead citrate and uranyl acetate. A Zeiss EM 900 electron microscope was used for examination and microphotographs were taken with a camera (Zeiss, Oberkochen, Germany).

Quantification of myelinated fibers

For the electron microscopy, five pictures each at ×7000, ×12,000, ×20,000, and ×30,000 magnification were analyzed by three blinded observers. Particles were counted in an area of 5.25 µm^2. Quantitative analysis was performed using the Mann-Whitney U test (StatviewII, Abacus, Berkeley, Calif.). The level of significance was set at $*P < 0.05$, $**P < 0.01$, $***P < 0.001$. Sections from the kidney served as negative controls.

For the densiometric measurements of the molecular layer of the DG after ECL, the slides were digitalized using a camera (Olympus BX-50, Hamburg, Germany). To quantify the intensity at a pixel level, we used the computerized videodensiometry system (Metamorph; Universal Imaging, Downingtown, PA.). A visually established pixel intensity threshold was set to remove the unlabeled portion of the image. A standard rectangle was defined and placed in the molecular layer of the DG (4 mm^2). A smaller defined rectangle was placed in the outer molecular layer (2 mm^2). The percentage of fiber intensity in the outer molecular layer compared to the entire molecular layer was calculated [39]. A mean value of two measurements of three to five animals from each survival stage after deafferentation was calculated and set in reference to the unlesioned controls (100%). Analyses were performed using the Mann-Whitney U-test (StatView II). The level of significance was set at $*P < 0.05$, $**P < 0.01$, $***P < 0.001$.

Results

First appearance of myelinated fibers in the hippocampus during development

We investigated the appearance of myelinated fibers from the early postnatal stages using the myelin marker Black Gold. Initially, at P5, a diffuse staining in the hippocampal area could be found, especially in the white matter regions such as the alveus and stratum radiatum (fig. $1A_1$). At the same developmental stage, the temporal cortex was devoid of any labeling. At P17, identifiable Black Gold-positive myelinated fibers appeared in the hippocampus (fig. 1B). Many myelinated fibers could be found in the strata oriens and radiatum of the CA regions and in the temporal cortex (fig. $1B_1$–B_3), but not in the molecular layer of the dentate gyrus (fig. $1B_1$). At P25, the number of myelinated fibers was significantly higher in comparison to earlier postnatal time points and showed no remarkable difference compared with the adult (fig. $1C_1$–C_3, D).

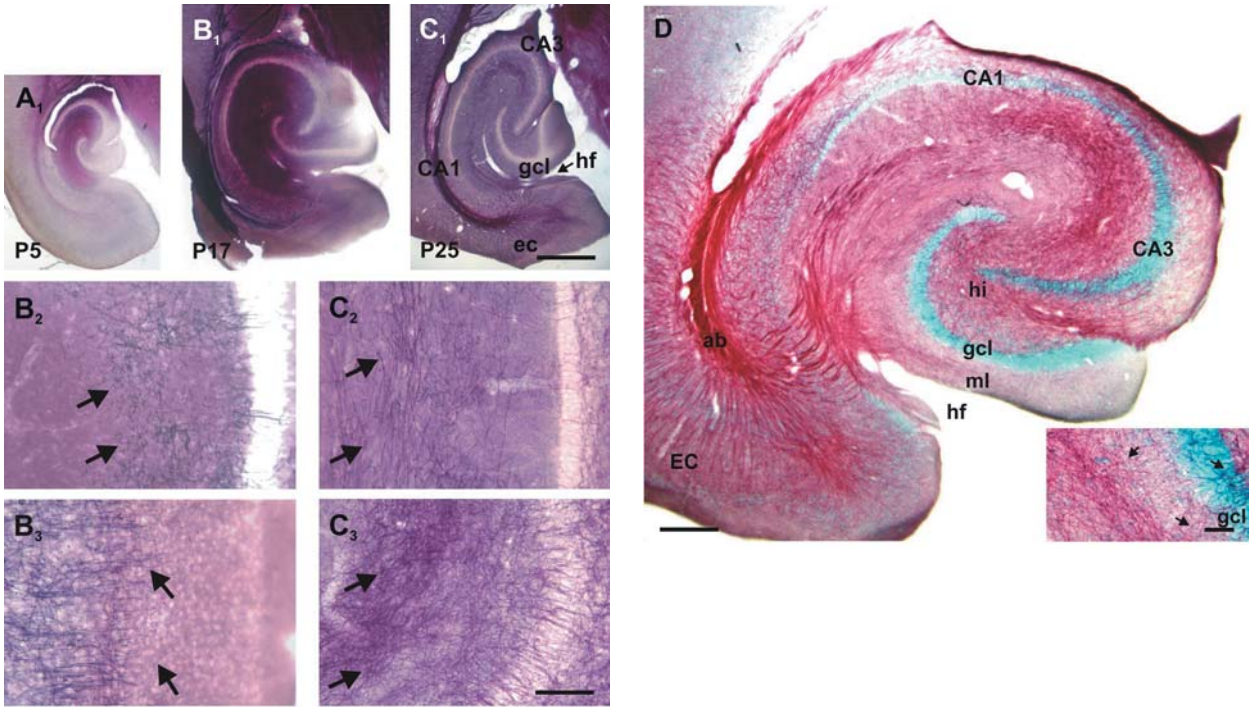

Figure 1. Appearance of mature axons during postnatal development and in the adult hippocampus. Black Gold-stained hippocampal sections at P5 (*A*), P17 (*B*), and P25 (*C*). High-power images were taken from survey micrographs from above. Discernible Black Gold (BG)-positive fibers are observed at P17 in the CA regions (B_2) as well as in the temporal cortex (B_3) (arrows). In addition, white-matter zones such as the angular bundle and the fornix are at that stage also strongly BG positive (B_1, C_1). Note that at this postnatal stage, entorhinal fibers already terminate in the DG. However, no BG-positive fibers could be found in the molecular layer at that stage (A_1–C_1). (*C*) At P25, fiber tracts of established afferents as well as intrinsic projections are clearly BG labeled as shown in the stratum lacunosum moleculare of the CA1 region (C_2) and in the CA3 region (C_3) (arrows). (*D*) Distribution of myelinated fibers in the adult hippocampus. BG-positive fibers are stained brown-red. Malachite green-counterstained neuronal cell bodies are BG negative. Note the prominent entorhinal projection running along the stratum lacunosum moleculare of the hippocampus proper. Many fibers cross the hippocampal fissure and invade the DG (arrows in the insert). In the stratum radiatum of the hippocampus, the Schaffer collaterals also stain intensively for BG. In addition, commissural fibers in the inner molecular layer are BG positive. (*A–D*) CA, cornu ammonis; gcl: granule cell layer; ml, molecular layer; hf, hippocampal fissure; ec, entorhinal cortex; ab, angular bundle. Scale bar in C_1 for all overview images: 800 µm; scale bar in C_3 for higher magnifications: 30 µm; scale bar in *D*: 900 µm; in the higher magnification of *D*: 20 µm.

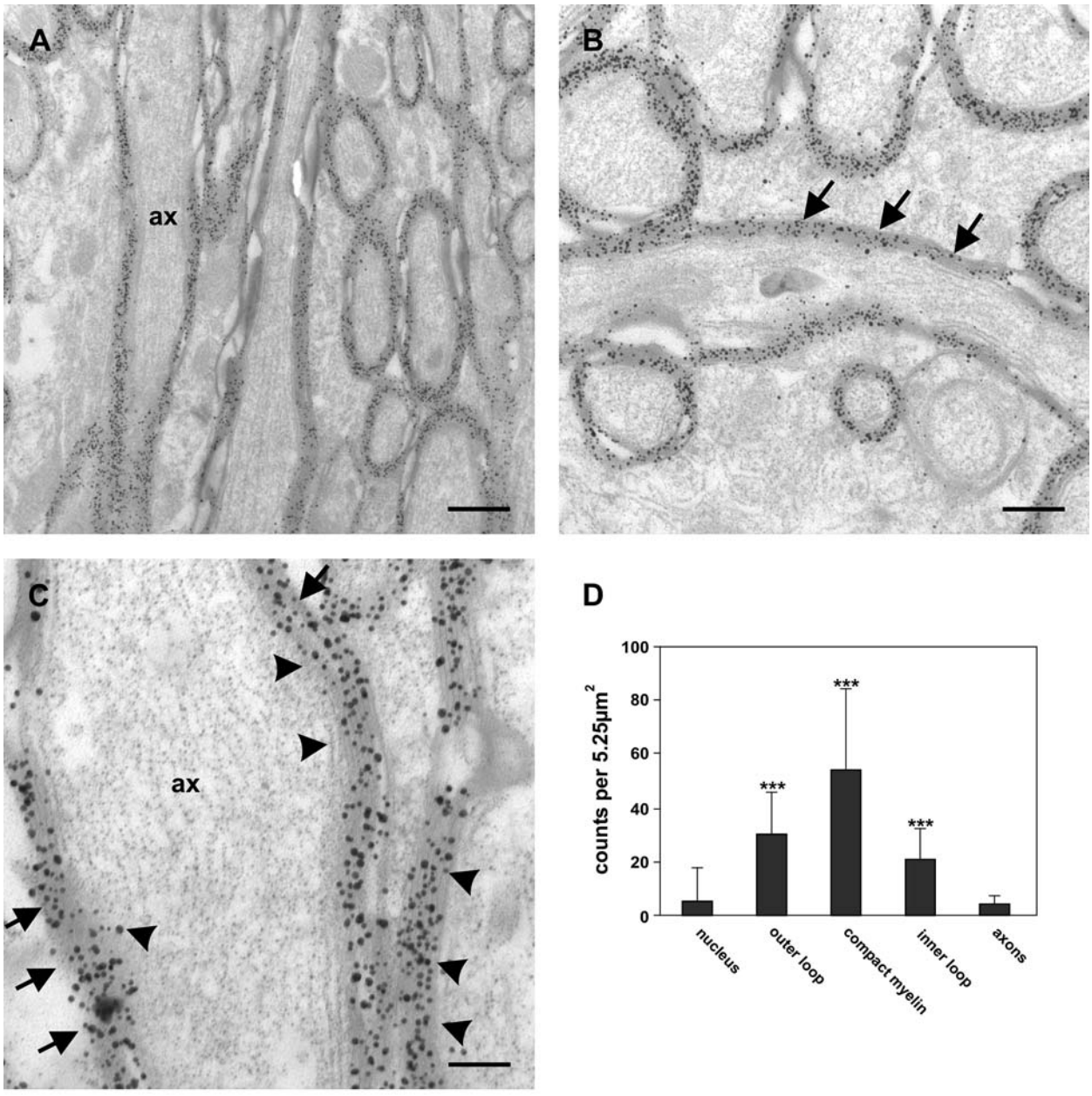

Figure 2. Ultrastructural localization of Black Gold (BG) in the hippocampus. Overview of BG particle distribution in the hilar region (*A*). Cell bodies were almost devoid of BG particles. BG particle distribution in the stratum radiatum of CA3 (*B*), higher magnification of the hilar region (*C*). BG particles are specifically arranged in myelin sheaths enveloping axons (ax). Arrows indicate the outer loop of myelin sheaths, arrowheads point to the inner myelin layer and axonal membranes. Quantification of the number of BG particles in different subcellular compartments (in the nucleus, outer loop, compact myelin, inner loop and axonal membrane, axoplasm) (*D*). Statistical differences are marked with asterisks (mean ± SD, * $P < 0.05$, ** $P < 0.01$, *** $P < 0.001$; measured with the Mann-Whitney U-test). Scale bar in A: 5 µm; in B: 3 µm; C: 0.6 µm.

Distribution of myelinated fibers in the adult hippocampus

A survey of the entorhino-hippocampal region showed the Black Gold-positive myeloarchitecture (fig. 1D). There, the perforant path traversing the hippocampal fissure is clearly visualized. After entering the white matter, the myelinated fibers pass the pyramidal cells of the subiculum and cross the hippocampal fissure to enter the outer molecular layer of the DG (fig. 1D). The main projections of the perforant path to the hippocampus terminate in the stratum lacunosum-moleculare. In addition, a fiber projection can be seen emerging from within the hilus, running through the stratum radiatum and lucidum of CA3, and ending at the CA2-CA1 border. The course of this projection in part resembles the mossy fiber projection, but apparently includes other fiber systems in the stratum radiatum (fig. 1D).

Ultrastructural analysis of myelination in the hippocampus

To address the question of whether the molecular substrate of Black Gold is indeed a protein component of myelin, we stained sections in which at least parts of proteins were diminished. In proteinase K- and trypsin-digested sections, Black Gold staining was abolished, whereas on the same sections, the staining by a common myelin marker, LFB, was unaffected in comparison to non-digested sections (data not shown). Analysis of the ultrastructural distribution of Black Gold staining in the hippocampus showed neither particles in the nucleus nor staining in the endoplasmatic reticulum (fig. 2). The majority of the particles were found in the compact myelin, most intensely in the inner and outer myelin layers surrounding mature axonal structures (fig. 2A–C). Cytoplasmic components of axons and dendritic processes did not show any significant Black Gold staining (fig. 2D). Interestingly, Black Gold has a high affinity for myelin proteins, which are located in the compact and inner and outer loops of myelin. This is significant since myelin proteins show a differential compartmentalization, i.e., MAG is mostly located in the inner myelin layers and myelin oligodendrocyte glycoprotein (MOG) in the outer myelin layer, whereas MBP is mainly concentrated in compact myelin [41]. Sections from kidney and liver, which are known not to express any myelin proteins, were completely devoid of Black Gold staining (data not shown).

Expression pattern of the myelin-specific markers MBP and MAG in the hippocampus

We next studied the expression pattern of myelinated fibers in the rat hippocampus by immunocytochemistry using antibodies against two major CNS myelin components, MBP and MAG. Both components showed essentially the same distribution pattern, although the signal for MBP was more intense (fig. 3). Immunoreactive

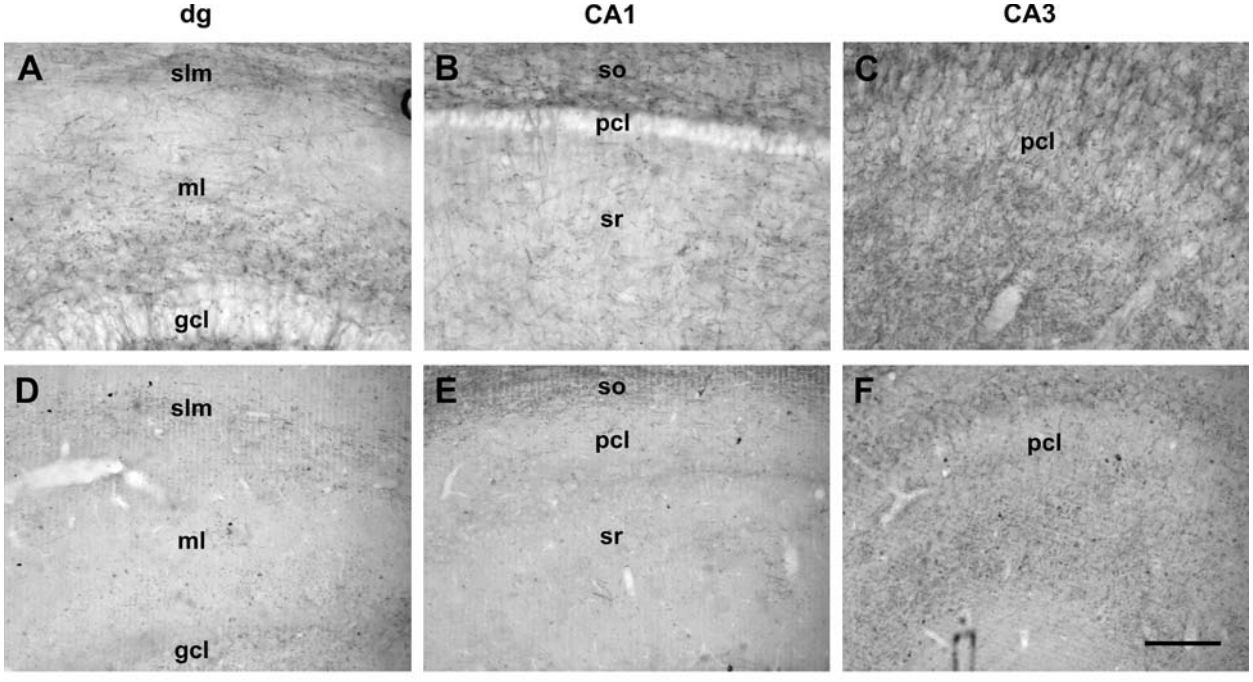

Figure 3. Immunostaining for MBP and MAG in the adult hippocampus. MBP-positive punctate staining is visible in the molecular layer of the DG and somewhat stronger in the inner third. The infragranular hilar region and the stratum lacunosum-moleculare of CA1 also show MBP immunolabeling (*A–C*). Although MAG immunoreactivity appears to be weaker than MBP (*D–F*), the distribution patterns of both myelin marker proteins are similiar. dg, dentate gyrus; CA, cornu ammonis; slm, stratum lacunosum-moleculare; ml, molecular layer; gcl, granule cell layer; sr, stratum radiatum; so, stratum oriens. Scale bar: 25 µm.

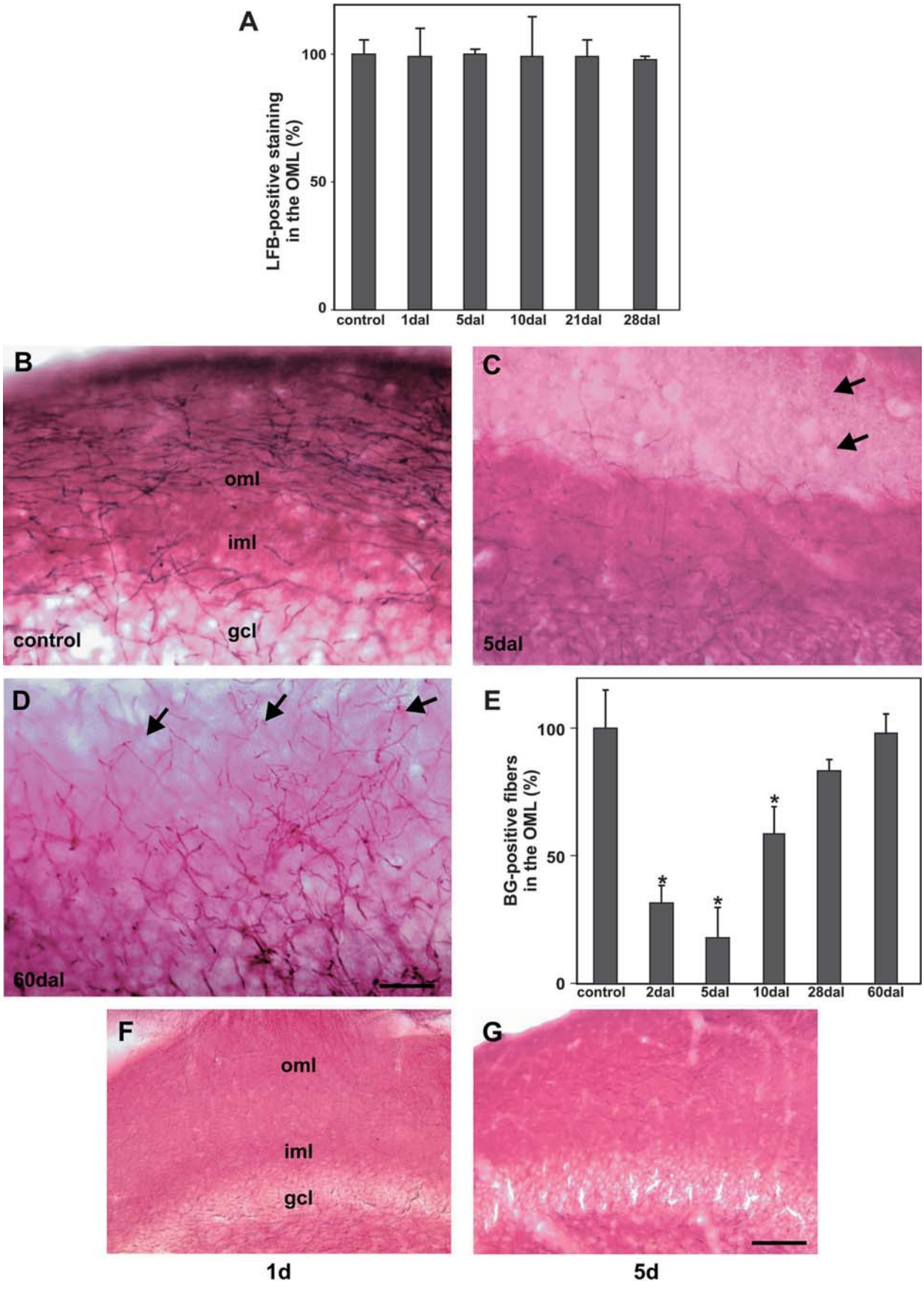
A
LFB-positive staining in the OML (%)
100
50
0
control
1dal
5dal
10dal
21dal
28dal
B
oml
iml
gcl
control
C
5dal
D
60dal
E
BG-positive fibers in the OML (%)
100
50
0
*
*
*
control
2dal
5dal
10dal
28dal
60dal
F
oml
iml
gcl
1d
G
5d

products were found in the strata radiata and lacunosum-moleculare as well as in the molecular layer of the DG [20, 34].

Loss and reappearance of myelin after deafferentation and seizure

We first investigated the distribution of myelin in the lesioned hippocampus with LFB (fig. 4A). In adult non-lesioned controls, LFB-positive myelin staining was visible in the alveus, stratum oriens, and in the corpus callosum. The LFB staining in the inner and outer molecular layers of the DG was weak, probably due to the low myelin content in contrast to the corpus callosum. Transection of the perforant path resulted in a loss of myelinated fiber especially in the outer molecular layer, a termination zone of entorhinal axons. However, no alteration in the LFB staining pattern could be detected in the hippocampus following lesion (fig. 4A). Using Black Gold, we were able to detect single myelinated fibers in the molecular layer of the adult DG (fig. 4B). Five days after ECL, the outer molecular layer was almost free of Black Gold-positive fibers (fig. 4C, E). Ten days after lesion, the first Black Gold-positive fibers reappeared in the outer molecular layer (fig. 4E). At longer survival stages, i.e., 28 and 60 days after lesion, the amount of myelinated fibers in the denervated zone reached control levels (fig. 4D, E). In another lesion paradigm, ECS were induced to produce increased neuronal activity and oligodendrocytic cell death [25–27, 42]. One day after ECS, myelinated fibers disappeared in the entire molecular layer of the DG and the gray matter of the temporal cortex (fig. 4F). In contrast, cortical and white-matter regions not directly affected showed no obvious changes in myelination (data not shown). The reoccurrence of Black Gold-positive fibers was found 5 days after seizures in the outer molecular layer as well as in the gray matter of the temporal cortex (fig. 4G).

Appearance of pathological myelin after lesion

Despite the fact that myelinated fibers disappeared in the outer molecular layer of the DG following lesion, pathological myelin structures were also found in the denervated zone (fig. 5). There, terminal tumescences and varicosities appeared along the distal segments of axotomized fibers (fig. 5B, C). Anterograde degenerated fibers showed a blurred delineation and bead-like varicosities along their distal segments (fig. 5C), features never observed in control sections.

Discussion

Using different markers for myelin, we investigated the appearance of myelin at the single fiber level in the hippocampus during development and following lesion. During development, axons invade the hippocampus at late embryonic stages [43–45], whereas myelination commences at P15 and is completed at P60 [20]. Following axotomy, a specific anterograde degeneration takes place in the hippocampus, accompanied by the loss of myelinated fibers and the appearance of pathological myelin structures. Time course studies revealed that the axonal sprouting response following brain lesion is quantitatively well correlated with reoccurring myelinated fibers [23].

Methodological considerations on myelination in the CNS

Studies of myelin in the CNS based on histochemical techniques have to be interpreted with some caution, as results may be influenced by the following factors: signal-to-noise ratio; considerable variability in staining; staining of unknown molecular substrate; and complex multi-step prestaining procedures. Therefore, we tested the modified gold chloride dye Black Gold developed by Schmued and Slikker [46] at the light and ultrastructural level and corroborated the Black Gold staining with established techniques. Black Gold staining at the light-microscopic level revealed myelin at single-fiber resolution. Furthermore, proteinase K digestion of brain sections prior to Black Gold staining indicated that Black Gold specifically stains protein compounds of myelin, in contrast to LFB, which binds with high affinity to non-solvent phospholipids [47]. In addition, electron microscopy revealed that Black Gold-stained myelin proteins are specifically present in all compartments of myelin sheaths, i.e., in compact myelin as well as in the inner and outer myelin loops. This is relevant, since myelin proteins show different compartmentalization, i.e., MAGs and Nogo-A are located in the inner loop of myelin sheaths [41].

Figure 4. Myelinated fibers in the molecular layer of the DG after lesion. Following lesion, no alterations in LFB staining could be detected (*A*). The percentage of LFB signal intensity of the outer molecular layer in comparison to the entire molecular layer of the DG is shown (*A*). BG-positive fibers are randomly distributed throughout the entire molecular layer in adult controls (*B*). At 5 days after lesion (5dal), the outer molecular layer appears to be free of BG-stained axonal processes (arrows) (*C*, *E*). The number of BG-positive fibers (arrows) in the molecular layer increases from 10dal onwards and reaches control levels at 60dal (*D*). Quantitative analysis of BG-positive fibers in the molecular layer from controls and lesioned animals at different postlesion time points (*E*). The percentage of signal intensity of the outer molecular layer is shown. BG staining after ECS (*F*, *G*). Note that nearly no myelinated fibers are present in the inner and outer molecular layers of the DG 1 day after seizure (*F*). Myelinated fibers reoccur 5 days after seizure in the molecular layer (*G*). Statistical differences are marked with asterisks (mean ± SD, * $P < 0.05$, ** $P < 0.01$, *** $P < 0.001$, measured with the Mann-Whitney U-test). gcl, granule cell layer, iml, inner molecular layer; oml, outer molecular layer. Scale bar in *C* (for *A–C*): 10 µm. Scale bar in *G* (for *F*, *G*): 50 µm.

Therefore, we are convinced that Black Gold-stained myelinated fibers represent at least the majority of myelinated fibers, and that Black Gold is therefore a suitable marker for detecting myelinated fibers in the CNS at the light and electron microscopy level.

Myelination in the hippocampus is temporally ordered during development

During development, axons invade the hippocampus and form a specific and segregated connection [43]. This hippocampal innervation is highly ordered and regulated by temporally expressed molecules rather than by a time-related competition for synaptic contacts [44, 48; for a review see ref. 49]. One major excitatory input originates from layer 2/3 of the entorhinal cortex and arrives at the hippocampus during late embryonic stages, segregating in a layer-specific manner in the outermost part of the DG (outer molecular layer) and CA1–CA3 region [19, 43, 49]. Commissural and septal projections first reach the hippocampus and DG perinatally, whereas associational projections are developed postnatally in the hippocampus [19, 50–52]. Expression of oligodendrocyte-specific genes such as MBP, Nogo-A and its isoforms, and MAG appears in the hippocampus at early postnatal stages [20, 34, 53]. However, Black Gold-positive fibers and ultrastructurally identified multilamellar and spirally wrapped structures were not found until P17 in the hippocampus. The fact that other white-matter regions also show Black Gold-positive fibers at earlier postnatal stages (P5) indicates that factors other than technical reasons may contribute to this phenomenon (fig. 1). One could speculate that neuronal activity influences the myelination and therefore accounts for the temporal delay between myelin-specific protein expression and the appearance of fully mature myelin structures. This idea is supported by the observation that myelinogenesis is induced by neuronal action potentials [54]. In the adult, entorhinal axons terminating in the outer molecular layer, which is known to be myelinated, could be clearly stained for Black Gold [55] (fig. 6).

To our surprise, we observed intense Black Gold labeling under light and electron microscopy resolutions not only in the stratum radiatum, which is occupied by commissural myelinated fibers, but also in the stratum lucidum. This lamina just above the somata of CA3 pyramidal cells is traversed by the mossy fiber tract, a projection hitherto regarded to be non-myelinated [18, 32, 52]. This observation suggests that numerous myelinated fibers of various origin may pass through this lamina. In addition, we found several myelin sheaths and myelinated axons in the hilar region. Since we cannot at this stage define the origin of those myelinated fibers, future studies combining selective axonal tracing and ultrastructural analysis should address these questions.

Myelination in the hippocampus following lesion and seizure

The time course of Black Gold-positive fiber expression following lesion reflected well the axonal degeneration and regeneration phases following lesion (fig. 6). The early postlesional stage in the hippocampus is characterized by Wallerian degeneration of entorhinal axons and the site-specific migration and activation of microglial and astroglial cells [56–59]. Conversely, the disappear-

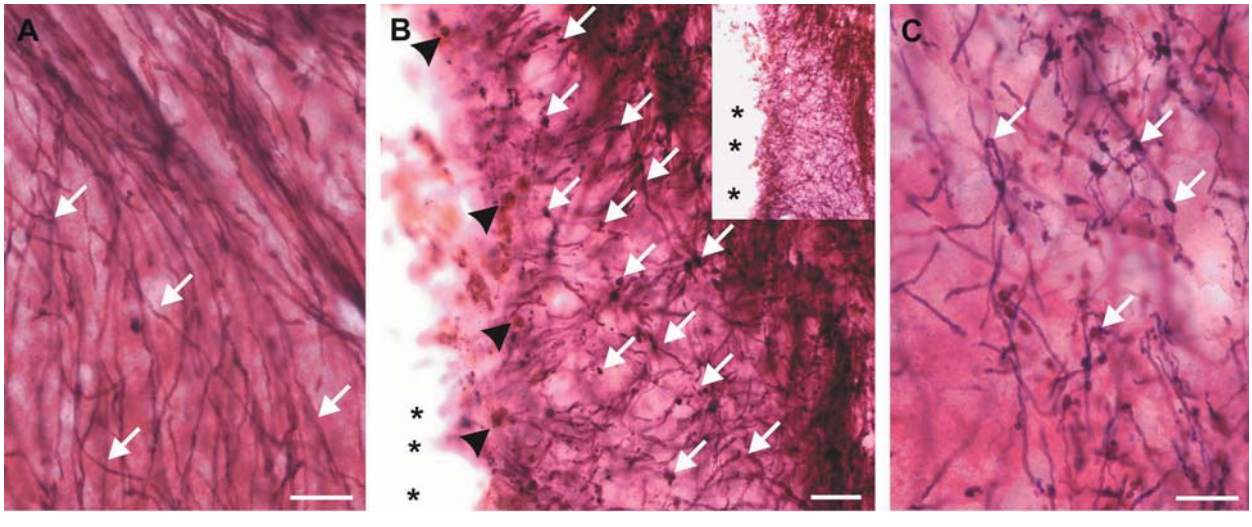

Figure 5. Lesion-induced myelin pathologies in the hippocampus revealed by Black Gold. (*A*) A high magnification of the entorhinal cortex from an adult control. The arrows indicate sharply outlined myelinated fibers. Scale bar: 10 µm. (*B*) Ten days after lesion, varicosities and bubbled myelin fibers are present in the affected zone. The corresponding overview is given as insert. Asterisks mark the transection site. Arrowheads show invaded blood cells in close vicinity to the lesion site. Scale bar: 21 µm. (*C*) Bubbles of pathological myelin (arrows) appear as bead-like varicosities along the severed axonal remnants (high magnification of *B*). Scale bar: 7 µm.

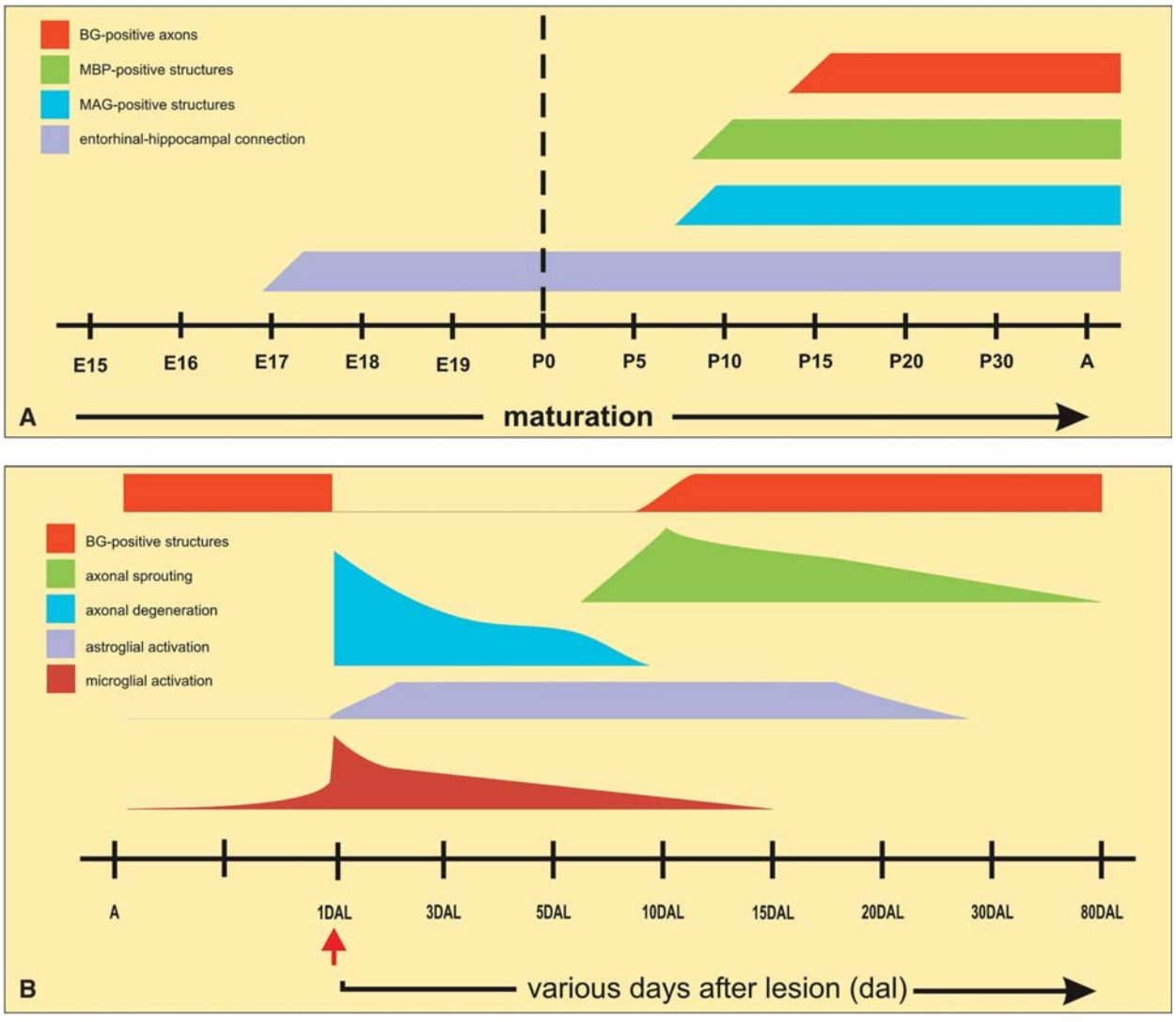

Figure 6. Summary of Black Gold staining results during development and following lesion. (*A*) Scheme of the development of the entorhinal-hippocampal connection. First, entorhinal axons invade the hippocampus at E17, and in the second postnatal week this connection is fully developed. Oligodendrocyte-specific markers (MBP, MAG) are first expressed in the hippocampus at P10. Black Gold-positive fibers are first detectable at P17. A, adult. (*B*) Summary of myelin-specific staining results and events following brain lesion in the hippocampus. Immediately after lesion, Black Gold-positive fibers decline and pathological myelin stuctures appear in the affected regions. These results correlate with the process of Wallerian degeneration and microglial and astroglial activation and phagocytotic activity. The onset of reappearing Black Gold-positive fibers starts at 10 days after lesion (10dal) and reaches control levels at 28dal. This time course corresponds well to the axonal sprouting phase and the readjusted electrophysiological balance after lesion. Note, that no alteration of LFB staining could be detected in the hippocampus following lesion. A, adult.

ance of stained myelinated fibers corresponds well to the anterograde degeneration phase taking place following lesion [56]. Therefore, the decline of Black Gold-positive axons in the DG is in line with the decreased synaptic input following lesion [35]. The decline in Black Gold staining reached its lowest level at 5 days after lesion, a time point when neurodegeneration processes are at their peak and glial phagocytotic activity is at its maximum [58, 60, 61] (fig. 6). Noteworthy in this context is that MBP expression has been shown to correlate inversely with the microglial activation in this lesion paradigm [62] and in cuprizone-induced demyelination [63].

During the phase when axon sprouting and outgrowth begins, increased Black Gold-positive fibers could be found in the outer molecular layer [64–66]. Longer survival stages revealed Black Gold-positive fiber density comparable to adult non-lesioned controls. This time course is also seen with acetylcholinesterase (AChE) histochemistry, which is generally used for demonstrating lesion-induced sprouting [67, 68]. In addition to the detection of a subpopulation of sprouting fibers, i.e., AChE-positive fibers, the advantage of Black Gold is its ability to detect the entire population of myelinated fibers, regardless of their origin. The quantitative analysis of myelinated fibers

in longer survival stages effectively reflects the readjusted axonal density and electrophysiological balance following lesion [36, 69] (fig. 6). However, future studies using combined axonal tracing and myelin-staining procedures will need to answer the question whether the reappearing Black Gold-positive fibers are a result of axon sprouts or of newly myelinated axons (that is, axons which are not normally myelinated). Compared to Black Gold, using the LFB dye as an established procedure for myelin staining did not result in the detection of lesion-induced changes. The reason for this could be, on the one hand, the relatively small proportion of myelinated fibers in relation to the total amount of myelin, which falls under the detection limit of LFB. On the other hand, LFB staining in the hippocampus is quite weak and far below single-fiber resolution. Thus, even qualitative changes in myelin content may remain unrecognized by LFB staining.

To confirm our results from the entorhinal cortex lesion paradigm, we tested Black Gold staining in the ECS model. In this approach, we observed a transient disappearance of myelinated fibers in the affected regions. Experimentally induced excessive neuronal activity (electroconvulsion, kainic acid, pilocarpine, pentylenetetrazole) is known to lead to glial activation and increased glutamate levels [24, 70, 71]. These events also affect and destroy myelin-forming oligodendrocytes through excitatory cell stress, a phenomenon which might be mirrored by the decrease in Black Gold staining [25–27]. The reappearance of myelinated fibers in this seizure model correlates with the appearance of the axonal sprouting marker GAP-43 [72].

In summary, our results show that myelination takes place in the highly plastic brain region in a temporal order during development. The occurrence of multilamellar, mature myelin structures in the hippocampus commences after the expression of myelin-specific proteins. Following lesion, the disappearance and reappearance of myelinated fibers correlates well with the degeneration and reorganization phase in the affected brain region. Thus, our results indicate that the process of myelination differs between development and lesion and that postlesional remyelination progresses in parallel with the axon-sprouting phase independently of the underlying disease.

Acknowledgements. We thank S. Lewandowski and D. Wachenschwanz for photographic and digital assistance. B. Mannfeld is acknowledged for rapid computational art work. D. Lajkó and G. Duwe are acknowledged for their excellent technical support. Many thanks to K. Rosegger and A. Mason for editorial work and suggestions on the manuscript. This study was supported by grants from the German Research Council (SFB 515/A5, SFB 505/A3, and DFG He-1520/2-1). N. E. S. is an Investigator of the Charité Medical Research Foundation (Habilitationsstipendium).

1 Richardson P. M., McGuinness U. M. and Aguayo A. J. (1980) Axons from CNS neurons regenerate into PNS grafts. Nature **284:** 264–265
2 David S. and Aguayo A. J. (1981) Axonal elongation into peripheral nervous system 'bridges' after central nervous system injury in adult rats. Science **214:** 931–933
3 Caroni P. and Schwab M. E. (1988) Two membrane protein fractions from rat central myelin with inhibitory properties for neurite growth and fibroblast spreading. J. Cell Biol. **106:** 1281–1288
4 Caroni P. and Schwab M. E. (1988) Antibody against myelin-associated inhibitor of neurite growth neutralizes nonpermissive substrate properties of CNS white matter. Neuron **1:** 85– 96
5 Savio T. and Schwab M. E. (1990) Lesioned corticospinal tract axons regenerate in myelin-free rat spinal cord. Proc. Natl. Acad. Sci. USA **87:** 4130–4133
6 Schnell L. and Schwab M. E. (1990) Axonal regeneration in the rat spinal cord produced by an antibody against myelin-associated neurite growth inhibitors. Nature **343:** 269–272
7 Kapfhammer J. P. and Schwab M. E. (1992) Modulators of neuronal migration and neurite growth. Curr. Opin. Cell Biol. **4:** 863–868
8 McKerracher L., David S., Jackson D. L., Kottis V., Dunn R. J. and Braun P. E. (1994) Identification of myelin-associated glycoprotein as a major myelin-derived inhibitor of neurite growth. Neuron **13:** 805–811
9 Mukhopadhyay G., Doherty P., Walsh F. S., Crocker P. R. and Filbin M. T. (1994) A novel role for myelin-associated glycoprotein as an inhibitor of axonal regeneration. Neuron **13:** 757–767
10 Wang K. C., Koprivica V., Kim J. A., Sivasankaran R., Guo Y., Neve R. L. et al. (2002) Oligodendrocyte-myelin glycoprotein is a Nogo receptor ligand that inhibits neurite outgrowth. Nature **417:** 941–944
11 Dou C. L. and Levine J. M. (1994) Inhibition of neurite growth by the NG2 chondroitin sulfate proteoglycan. J. Neurosci. **14:** 7616–7628
12 Niederost B. P., Zimmermann D. R., Schwab M. E. and Bandtlow C. E. (1999) Bovine CNS myelin contains neurite growth-inhibitory activity associated with chondroitin sulfate proteoglycans. J. Neurosci. **19:** 8979–8989
13 Chen M. S., Huber A. B., Haar M. E. van der, Frank M., Schnell L., Spillmann A. A. et al. (2000) Nogo-A is a myelin-associated neurite outgrowth inhibitor and an antigen for monoclonal antibody IN-1. Nature **403:** 434–439
14 GrandPre T., Nakamura F., Vartanian T. and Strittmatter S. M. (2000) Identification of the Nogo inhibitor of axon regeneration as a Reticulon protein. Nature **403:** 439–444
15 Prinjha R., Moore S. E., Vinson M., Blake S., Morrow R., Christie G. et al. (2000) Inhibitor of neurite outgrowth in humans. Nature **403:** 383–384
16 Henderson Z., Morris N. P., Grimwood P., Fiddler G., Yang H. W. and Appenteng K. (2001) Morphology of local axon collaterals of electrophysiologically characterised neurons in the rat medial septal/diagonal band complex. J. Comp. Neurol. **430:** 410–432
17 Coetzee T., Fujita N., Dupree J., Shi R., Blight A., Suzuki K., Suzuki K. et al. (1996) Myelination in the absence of galactocerebroside and sulfatide: normal structure with abnormal function and regional instability. Cell **86:** 209–219
18 Frotscher M. and Leranth C. (1985) Cholinergic innervation of the rat hippocampus as revealed by choline acetyltransferase immunocytochemistry: a combined light and electron microscopic study. J. Comp. Neurol. **239:** 237–246
19 Super H. and Soriano E. (1994) The organization of the embryonic and early postnatal murine hippocampus. II. Development of entorhinal, commissural, and septal connections studied with the lipophilic tracer DiI. J. Comp. Neurol. **344:** 101–120

20 Savaskan N. E., Plaschke M., Ninnemann O., Spillmann A. A., Schwab M. E., Nitsch R. et al. (1999) Myelin does not influence the choice behaviour of entorhinal axons but strongly inhibits their outgrowth length in vitro. Eur. J. Neurosci. **11:** 316–326

21 Savaskan N. E., Eyupoglu I. Y., Brauer A. U., Plaschke M., Ninnemann O., Nitsch R. et al. (2000) Entorhinal cortex lesion studied with the novel dye fluoro-jade. Brain Res. **864:** 44–51

22 Frotscher M., Heimrich B. and Deller T. (1997) Sprouting in the hippocampus is layer-specific. Trends Neurosci. **20:** 218–223

23 Savaskan N. E. and Nitsch R. (2001) Molecules involved in reactive sprouting in the hippocampus. Rev. Neurosci. **12:** 195–215

24 Chapman A. G., Westerberg E., Premachandra M. and Meldrum B. S. (1984) Changes in regional neurotransmitter amino acid levels in rat brain during seizures induced by L-allylglycine, bicuculline, and kainic acid. J. Neurochem. **43:** 62–70

25 Pitt W., Werner P. and Raine C. S. (2000) Glutamate excitotoxicity in a model of multiple sclerosis. Nat. Med. **6:** 67–70

26 Smith P. M. and Blakemore W. F. (2000) Porcine neural progenitors require commitment to the oligodendrocyte lineage prior to transplantation in order to achieve significant remyelination of demyelinated lesions in the adult CNS. Eur. J. Neurosci. **12:** 2414–2424

27 Matute C., Alberdi E., Domercq M., Perez-Cerda F., Perez-Samartin A. and Sanchez-Gomez M. V. (2001) The link between excitotoxic oligodendroglial death and demyelinating diseases. Trends Neurosci. **24:** 224–230

28 Scott B. W., Wojtowicz J. M. and Burnham W. M. (2000) Neurogenesis in the dentate gyrus of the rat following electroconvulsive shock seizures. Exp. Neurol. **165:** 231–236

29 Vaidya V. A., Siuciak J. A., Du F. and Duman R. S. (1999) Hippocampal mossy fiber sprouting induced by chronic electroconvulsive seizures. Neuroscience **89:** 157–166

30 Amaral D. G. (1978) A Golgi study of cell types in the hilar region of the hippocampus in the rat. J. Comp. Neurol. **182:** 851–914

31 Bayer S. A. and Altman J. (1987) Directions in neurogenetic gradients and patterns of anatomical connections in the telencephalon. Prog. Neurobiol. **29:** 57–106

32 Berger T. and Frotscher M. (1994) Distribution and morphological characteristics of oligodendrocytes in the rat hippocampus in situ and in vitro: an immunocytochemical study with the monoclonal Rip antibody. J. Neurocytol. **23:** 61–74

33 Kapfhammer J. P. and Schwab M. E. (1994) Increased expression of the growth-associated protein GAP-43 in the myelin-free rat spinal cord. Eur. J. Neurosci. **6:** 403–411

34 Suzuki M. and Raisman G. (1994) Multifocal pattern of postnatal development of the macroglial framework of the rat fimbria. Glia **12:** 294–308

35 Campagnoni A. T. and Macklin W. B. (1988) Cellular and molecular aspects of myelin protein gene expression. Mol. Neurobiol. **2:** 41–89

36 Brauer A. U., Savaskan N. E., Kole M. H., Plaschke M., Monteggia L. M., Nestler E. J. et al. (2001) Molecular and functional analysis of hyperpolarization-activated pacemaker channels in the hippocampus after entorhinal cortex lesion. FASEB J. **15:** 2689–2701

37 Brauer A. U., Savaskan N. E., Plaschke M., Ninnemann O. and Nitsch R. (2003) Cholecystokinin expression after hippocampal deafferentiation: molecular evidence revealed by differential display-reverse transcription-polymerase chain reaction. Neuroscience **121:** 111–121

38 Paxinos G., Watson C., Pennisi M. and Topple A. (1985) Bregma, lambda and the interaural midpoint in stereotaxic surgery with rats of different sex, strain and weight. J. Neurosci. Methods **13:** 139–143

39 Eyupoglu I. Y., Savaskan N. E., Brauer A. U., Nitsch R. and Heimrich B. (2003) Identification of neuronal cell death in a model of degeneration in the hippocampus. Brain Res. Brain Res. Protoc. **11:** 1–8

40 Borchert A., Savaskan N. E. and Kuhn H. (2003) Regulation of expression of the phospholipid hydroperoxide/sperm nucleus glutathione peroxidase gene: tissue-specific expression pattern and identification of functional cis- and trans-regulatory elements. J. Biol. Chem. **278:** 2571–2580

41 Huber A. B., Weinmann O., Brosamle C., Oertle T. and Schwab M. E. (2002) Patterns of Nogo mRNA and protein expression in the developing and adult rat and after CNS lesions. J. Neurosci. **22:** 3553–3567

42 Cole A. J., Abu-Shakra S., Saffen D. W., Baraban J. M. and Worley P. F. (1990) Rapid rise in transcription factor mRNAs in rat brain after electroshock-induced seizures. J. Neurochem. **55:** 1920–1927

43 Skutella T., Savaskan N. E., Ninnemann O. and Nitsch R. (1999) Target- and maturation-specific membrane-associated molecules determine the ingrowth of entorhinal fibers into the hippocampus. Dev. Biol. 211: 277–292

44 Stein E., Savaskan N. E., Ninnemann O., Nitsch R., Zhou R. and Skutella T. (1999) A role for the Eph ligand ephrin-A3 in entorhino-hippocampal axon targeting. J. Neurosci. **19:** 8885– 8893

45 Steup A., Ninnemann O., Savaskan N. E., Nitsch R., Puschel A. W. and Skutella T. (1999) Semaphorin D acts as a repulsive factor for entorhinal and hippocampal neurons. Eur. J. Neurosci. **11:** 729–734

46 Schmued L. and Slikker W. Jr (1999) Black-gold: a simple, high-resolution histochemical label for normal and pathological myelin in brain tissue sections. Brain Res. **837:** 289–297

47 Kluver H. and Barrera E. (1953) A method for the combined staining of cells and fibers in the nervous system. J. Neuropathol. Exp. Neurol. **12:** 400–403

48 Frotscher M. and Heimrich B. (1993) Formation of layer-specific fiber projections to the hippocampus in vitro. Proc. Natl. Acad. Sci. USA **90:** 10400–10403

49 Skutella T. and Nitsch R. (2001) New molecules for hippocampal development. Trends Neurosci. **24:** 107–113

50 Fricke R. and Cowan W. M. (1977) An autoradiographic study of the development of the entorhinal and commissural afferents to the dentate gyrus of the rat. J. Comp. Neurol. **173:** 231–250

51 Ribak C. E., Seress L. and Amaral D. G. (1985) The development, ultrastructure and synaptic connections of the mossy cells of the dentate gyrus. J. Neurocytol. **14:** 835–857

52 Frotscher M. (1991) Target cell specificity of synaptic connections in the hippocampus. Hippocampus **1:** 123–130

53 Meier S., Brauer A. U., Heimrich B., Schwab M. E., Nitsch R. and Savaskan N. E. (2003) Molecular analysis of Nogo expression in the hippocampus during development and following lesion and seizure. FASEB J. **17:** 1153–1155

54 Demerens C., Stankoff B., Logak M., Anglade P., Allinquant B., Couraud F. et al. (1996) Induction of myelination in the central nervous system by electrical activity. Proc. Natl. Acad. Sci. USA **93:** 9887–9892

55 Nafstad P. H. (1967) An electron microscope study on the termination of the perforant path fibres in the hippocampus and the fascia dentata. Z. Zellforsch. Mikrosk. Anat. **76:** 532–542

56 Savaskan N. E., Skutella T., Brauer A. U., Plaschke M., Ninnemann O. and Nitsch R. (2000) Outgrowth-promoting molecules in the adult hippocampus after perforant path lesion. Eur. J. Neurosci. **12:** 1024–1032

57 Kawaja M. D. and Gage F. H. (1991) Reactive astrocytes are substrates for the growth of adult CNS axons in the presence of elevated levels of nerve growth factor. Neuron **7:** 1019–1030

58 Bechmann I. and Nitsch R. (1997) Astrocytes and microglial cells incorporate degenerating fibers following entorhinal lesion: a light, confocal, and electron microscopical study using a phagocytosis-dependent labeling technique. Glia **20:** 145– 154

59 Eyupoglu I. Y., Bechmann I. and Nitsch R. (2003) Modification of microglia function protects from lesion-induced neuronal al-

terations and promotes sprouting in the hippocampus. FASEB J. **17:** 1110–1111
60 Gall C., Rose G. and Lynch G. (1979) Proliferative and migratory activity of glial cells in the partially deafferented hippocampus. J. Comp. Neurol. **183:** 539–549
61 Jensen J. B. and Mork A. (1997) Altered protein phosphorylation in the rat brain following chronic lithium and carbamazepine treatments. Eur. Neuropsychopharmacol. **7:** 173– 179
62 Jensen M. B., Poulsen F. R. and Finsen B. (2000) Axonal sprouting regulates myelin basic protein gene expression in denervated mouse hippocampus. Int. J. Dev. Neurosci. **18:** 221–235
63 Morell P., Barrett C. V., Mason J. L., Toews A. D., Hostettler J. D., Knapp G. W. et al. (1998) Gene expression in brain during cuprizone-induced demyelination and remyelination. Mol. Cell Neurosci. **12:** 220–227
64 Cotman C., Gentry C. and Steward O. (1977) Synaptic replacement in the dentate gyrus after unilateral entorhinal lesion: electron microscopic analysis of the extent of replacement of synapses by the remaining entorhinal cortex. J. Neurocytol. **6:** 455–464
65 Matthews D. A., Cotman C. and Lynch G. (1976) An electron microscopic study of lesion-induced synaptogenesis in the dentate gyrus of the adult rat. I. Magnitude and time course of degeneration. Brain Res. **115:** 1–21
66 Matthews D. A., Cotman C. and Lynch G. (1976) An electron microscopic study of lesion-induced synaptogenesis in the dentate gyrus of the adult rat. II. Reappearance of morphologically normal synaptic contacts. Brain Res. **115:** 23–41
67 Mesulam M. M., Mufson E. J. and Rogers J. (1987) Age-related shrinkage of cortically projecting cholinergic neurons: a selective effect. Ann. Neurol. **22:** 31–36
68 Kugler P., Schleicher A., Zilles K. and Horvath E. (1993) Acetylcholinesterase activity and post-lesional plasticity in the hippocampus of young and aged rats. Neuroscience **55:** 91– 103
69 Clusmann H., Nitsch R. and Heinemann U. (1994) Long lasting functional alterations in the rat dentate gyrus following entorhinal cortex lesion: a current source density analysis. Neuroscience **61:** 805–815
70 Wade J. V., Samson F. E., Nelson S. R. and Pazdernik T. L. (1987) Changes in extracellular amino acids during soman- and kainic acid-induced seizures. J. Neurochem. **49:** 645–650
71 Dobkin J. and Marton M. (1970) A new procedure for the measurement of acid-soluble glutamine of tissue with particular reference to the brain. J. Neurochem. **17:** 231–235
72 Bendotti C., Pende M. and Samanin R. (1994) Expression of GAP-43 in the granule cells of rat hippocampus after seizure-induced sprouting of mossy fibres: in situ hybridization and immunocytochemical studies. Eur. J. Neurosci. **6:** 509–515